RSC Advances

PAPER

View Article Online
View Journal | View Issue

Cite this: *RSC Adv.*, 2020, **10**, 44903

Investigation of PEG/mixed metal oxides as a new form-stable phase change material for thermoregulation and improved UV ageing resistance of bitumen

Suhong Zhu,[ab] Tao Ji,[a] Dongyu Niu[d] and Zhengxian Yang *[ac]

The form-stable phase change material (PCM), polyethylene glycol (PEG)/ZnMgAl-mixed metal oxides (MMO), is prepared as a performance-enhancing additive of bitumen. In PEG/MMO PCM, PEG exhibits the phase-change function while ZnMgAl-MMO acts as the support carrier to prevent leakage of liquid PEG during phase transition. The properties of PEG/MMO PCM were analysed by XRD, SEM, FTIR, DSC, TG and UV-vis spectrophotometry. The results showed that the maximum PEG confined by MMO could be 65% and 65PEG/MMO PCM exhibited good thermal and chemical stability, sufficient phase change enthalpy and excellent UV absorption properties. Furthermore, the temperature regulation and UV ageing resistance of PEG/MMO PCM modified bitumen was evaluated by the thermal storage and release test and accelerated UV aging test. As a new type of performance-enhancing additive, PEG/MMO PCM is expected to be effective in regulating extreme temperature and resisting UV aging of bitumen and thus significantly extending the service life of bitumen pavement.

Received 1st October 2020
Accepted 30th November 2020

DOI: 10.1039/d0ra08398d

rsc.li/rsc-advances

1. Introduction

In the past few decades, Phase Change Materials (PCMs) have been widely used in diverse fields based on their capacity to store or release thermal energy at a stable temperature or within a small temperature range during phase change.[1–3] It is a remarkable fact that the applications of PCMs in civil and structural engineering have been rapidly increased.[3,4] Mixing PCMs into cement concrete, plaster boards and masonry walls can regulate the indoor temperature, and thus contribute to energy conservation and environmental protection.[5–10] In recent years, PCMs have been also applied in bitumen mixtures to enhance the temperature adaptability, which helps reduce the temperature damage of bitumen and extend the service life of bitumen pavement.[2,11–13]

Due to the unique features including suitable phase change temperatures, sufficient phase change latent heat, good phase change cycle stability and certain high temperature resistant properties, polyethylene glycol (PEG) has received considerable attention for application as a PCM.[14–16] However, the commercial application of PEG mainly faces two problems: low thermal conductivity and phase instability in melting state. The latter particularly limits its viability greatly.[3] The direct incorporation of PEG in bitumen may increase the saturated content of bitumen, which will reduce the consistency of bitumen, resulting in higher penetration and lower ductility.[11] PEG-based form-stable PCMs which are often composed of PEG and supporting materials have been developed to overcome the shortcomings. These PEG-based form-stable PCMs such as PEG/silica,[17–20] PEG/diatomite,[21,22] PEG/gypsum,[23] PEG/montmorillonite,[24,25] PEG/porous carbons,[26–28] and PEG/polymers,[29–32] can keep the solid state even when PEG is undergoing solid–liquid phase transition above the melting temperatures. Additionally, Zhu *et al.*[33] prepared a PEG/surface-modified layered double hydroxides (LDHs) form-stable PCM using the surface-modified LDHs as supporting material to prevent leakage of liquid PEG. It was found that the PCM (PEG/KH-LDHs) exhibited more stable shape and considerable latent heat capacity than pure PEG.

Layered double hydroxides (LDHs) are known as a family of host–guest anionic clays with lamellar structures, which can be represented by the general formula $[M_{1-x}^{2+}M_x^{3+}(OH)_2]^{x+}A_{x/m}^{m-}\cdot nH_2O$, where M^{2+} and M^{3+} are divalent and trivalent metal cations and A^{m-} is the anions located in interlayer region along with water molecules.[34] According to previous studies, upon calcination of LDHs at moderate temperature, a mixed metal oxide (MMO) consisting of two or multi-metal oxide and a spinel-like phase can be obtained.[35,36] The resulting MMO material possesses many unique properties and can be used as

[a]*Fujian Provincial University Research Centre for Advanced Civil Engineering Materials, Fuzhou University, Fuzhou 350116, China*

[b]*Department of Civil and Building Engineering, Nanchang Institute of Technology, Nanchang 330099, China*

[c]*College of Civil Engineering, Fuzhou University, Fuzhou 350116, China. E-mail: zxyang@fzu.edu.cn; zhengxian.yang@gmail.com*

[d]*Engineering Research Center for Transportation Materials of the Ministry of Education, Chang'an University, Xi'an 710061, China*

photocatalytic material, absorbent, catalyst and catalyst support.[37] In particular, due to the high surface area and a homogeneous dispersion of metal cations, MMO has been reported to be a highly attractive adsorbent with various application.[38–42] Zhao *et al.*[35] reported that ZnO-based MMO material which was derived from the corresponding LDHs precursor showed greater effectiveness in absorbing and screening ultraviolet light than the commercial ZnO-based material due to high dispersion of the ZnO phase within the amorphous metal oxide phase. In this context, PEG/MMO PCM can be expected to be a very advantageous and promising form-stable PCM, in which ZnO-based MMO derived from calcination of the LDHs precursor acts as the supporting matrix to prevent leakage of PEG during the melting process. Moreover, PEG/MMO PCM can be recognized as a new form-stable PCM with dual function of storing and releasing latent heat (provided by PEG) as well as absorbing and screening ultraviolet light (provided by MMO).

Previous researchers have applied PEG-based PCMs in bitumen mixture to adjust the temperature of bitumen pavement depending on their capacity for thermal energy storage of PEG-based PCM.[11,13] It has been found that the aged bitumen led to the premature deterioration of bitumen pavement.[33] To improve the applicability of PEG-based PCM in bitumen mixture, this research aims at preparing a novel form-stable PCM (PEG/MMO) which can be applied in bitumen with dual function in road engineering. That is to say not only contribute to thermoregulation but also to improve UV ageing resistance of bitumen. The properties of the novel form-stable PCM were analysed by X-ray diffraction (XRD), scanning electron microscopy (SEM), Fourier transform infrared (FTIR), differential scanning calorimetry (DSC), thermogravimetric analysis (TG) and UV-vis spectrophotometer. Furthermore, the capacity of PEG/MMO PCM in terms of temperature regulation and UV ageing resistance of modified bitumen was evaluated by thermal storage and release test and accelerated UV aging test.

2. Experimental

2.1 Materials

PEG with molecular weight (2000) was purchased from Shanghai Macklin Biochemical Co. Ltd., ZnMgAl-LDHs were obtained from Tianjin Jinheng Lanhai Technology Co. Ltd., the bitumen (FREP 70#A), with a penetration of 66 (0.1 mm at 25 °C, 100 g and 5 s), a ductility of more than 15 cm (10 °C), a softening point of 48.0 °C, and a viscosity of 0.431 Pa s (135 °C), was supplied from Xiamen Sunlit Co. Ltd., China.

2.2 Preparation of ZnMgAl-MMO

ZnMgAl-LDHs samples were calcined at 500 °C for five hours with a heating rate of 5 °C min^{-1} in a muffle furnace. The calcined samples were denoted as ZnMgAl-MMO.

2.3 Preparation of PEG/MMO PCM

PEG/MMO PCM was prepared by the solution impregnation method. Typically, PEG was first dissolved in anhydrous ethanol for 10 min at 50 °C. Then under magnetic stirring, ZnMgAl-MMO was added into the prepared solution at the mass ratios of (PEG/MMO) 60/40, 65/35, 70/30. The magnetic stirring proceeded for 5 h at room temperature. Afterward, the mixed solution was placed into an oven at 80 °C for 24 h before being completely dried and cooled down to room temperature. The resulting PEG/MMO PCM was denoted as 60PEG/MMO, 65PEG/MMO, 70PEG/MMO, respectively. For the comparison purpose, a composite of which PEG and ZnMgAl-LDHs at a mass ratio 60/40 was obtained by the same procedure and denoted as 60PEG/LDHs.

2.4 Preparation of PEG/MMO PCM modified bitumen

PEG/MMO PCM modified bitumen was prepared by high shear mixer and the specific preparation method was as follows: base bitumen was heated to a fully fluid at around 140 °C. Then 7% proportion of PEG/MMO PCM was slowly added into base bitumen. The blend was mixed at shearing rate of 4500 rpm at 165 °C for 60 min to ensure distribute homogenously. Finally, the resulting modified bitumen was preserved for subsequent experiments and denoted as PMB. For the comparison purpose, base bitumen (BB) was treated with the same condition.

2.5 Thermal storage and release assessment

Before conducting the assessment, PEG/MMO PCM was added into base bitumen using high shear emulsifier. The modified bitumen in which the percentage of PEG/MMO PCM was 7% is denoted as PMB. A typical thermal storage and release assessment was carried out as following: 100 g base bitumen (BB) and 100 g PMB were put into two identical flasks and a thermocouple with an accuracy of 0.1 °C was placed in the centre of each flask. The flasks were placed in the air for temperature equilibrium and then were put into 80 °C thermostatical water bath. After reaching temperature equilibrium, they were placed again in the air until to room temperature. The temperature of sample was simultaneously recorded by the thermocouple per 10 seconds.

2.6 UV aging resistance assessment

The UV aging properties of BB and PMB samples were assessed during exposure in a thin film oven test (TFOT) at 60 °C with an UV lamp of 500 W for 7 days according to ASTM D1754. The thickness of bitumen film was 3.2 mm and the intensity of UV irradiation was 1.2 W m^{-2}.

2.7 Characterization

BET surface area and pore properties of the ZnMgAl-LDHs and ZnMgAl-MMO were characterized by N_2 adsorption–desorption technique (ASAP 2460, Micromeritics, USA). A field emission scanning electron microscope (FESEM, Nova NanoSEM 230) was applied to obtain morphological features of sample. X-ray diffraction (XRD) (DY5261/Xpert3, CEM, USA) was used to determine the crystallization properties of PEG, ZnMgAl-MMO and PEG/MMO PCM. The of XRD was performed with a scanning angle from 5° to 80° (2θ) using Cu Kα radiation ($\lambda = 1.54$ Å, wavelength). A Fourier transform infrared (FTIR) spectroscopy

(Nicolet iS50, USA) was applied to investigate the spectra of PCM and bitumen samples by using attenuated total reflectance (ATR) method. All spectra were obtained in wavenumber range of 400–4000 cm^{-1}. The melting–freezing temperatures and the enthalpy of PEG/MMO PCM were determined using a DSC (DSC214, Netzsch, Germany) under a high-purity nitrogen atmosphere. All measurements were made with a temperature range from 0 °C to 120 °C at 5 °C min^{-1} rate. The thermal stability was evaluated by TG under a nitrogen atmosphere with the temperature range from 25 °C to 600 °C at a heating rate of 10 °C min^{-1}. The UV-vis absorption of bitumen was studied using a UV-vis spectrophotometer (Cary 7000, Agilent, USA) in a range from 200 to 800 nm with a slit width of 2.0 nm.

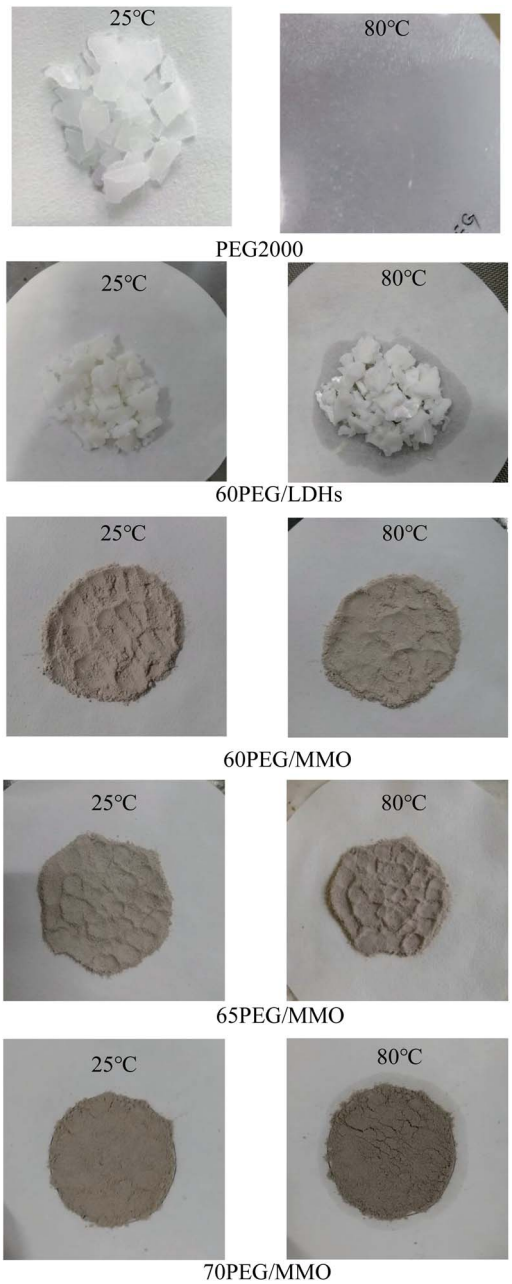

Fig. 1 Shape-stabilized property of a series of PEG-based PCMs at different temperatures.

3. Results and discussion

3.1 Stability of PEG/MMO PCM

Fig. 1 displays the state of a series of PEG-based PCMs at 25 °C and 80 °C. As can be seen, all samples are solid state at 25 °C, while at 80 °C, PEG2000 is completely converted to liquid state; 60PEG/LDHs and 70PEG/MMO have leakage of liquid PEG on the filter paper. In the cases of 60PEG/MMO and 65PEG/MMO, there are little exudation on the filter paper. It is well known that phase change can be occurred for PEG2000 from solid to liquid at around 50 °C. Thus, the fact that no leakage was found in 60PEG/MMO and 65PEG/MMO indicated that the leakage during phase change had be avoided using ZnMgAl-MMO as a support matrix. In this context, it is concluded that PEG/MMO can be a good form-stable PCM when the loadage fraction of PEG is below 65%. A possible reason for that can be attributed to the large specific surface area and pore structure properties of ZnMgAl-MMO. As is known that the calcination of LDHs can not only lead to changes of their structures, but also cause variation of their surface areas and pore structures.[41,43] Table 1 lists the BET surface area and pore structures of ZnMgAl-LDHs and ZnMgAl-MMO. As can be seen, the BET surface area and total pore volume of ZnMgAl-MMO are obviously larger than those of ZnMgAl-LDHs with the smaller average pore width. This observation can be explained that, upon calcination, the layered structures of LDHs are collapsed to small pieces, and then crystalline oxides phases form and pores appear due to the loss of water and anions.[44,45] The result implies that no leakage of PEG in PEG/MMO PCM is relevant to the increased surface area and pore development of MMO and physical adsorption and capillary force plays a significant role in maintaining the solid form of PEG/MMO PCM.

3.2 Morphology characterization by SEM

Fig. 2 shows the representative SEM images of ZnMgAl-LDHs (a, b), ZnMgAl-MMO (c, d) and 65PEG/MMO PCM (e, f). It can be seen that ZnMgAl-LDHs have sizes of hundreds nanometers with typically plate-like morphology and lamellar structures. ZnMgAl-MMO nanoplates display smaller crystal size and more irregular flake-morphology relative to ZnMgAl-LDHs owing to the collapse of the brucite-like layer upon calcination at 500 °C.[45] For 65PEG/MMO PCM, it can be seen that PEG has been absorbed on the surface of ZnMgAl-MMO, and the surface of ZnMgAl-MMO looks smoother than that one without PEG. The microstructure of 65PEG/MMO PCM clearly indicates the confinement of PEG by ZnMgAl-MMO, which contributes to the formation of a new form-stable PCM.

Table 1 BET and pore structure of ZnMgAl-LDHs and ZnMgAl-MMO

Sample	S_{BET} (m^2 g^{-1})	Pore volume (cm^3 g^{-1})	Adsorption average pore width (nm)
ZnMgAl-LDHs	24.165	0.043	7.103
ZnMgAl-MMO	187.659	0.216	4.614

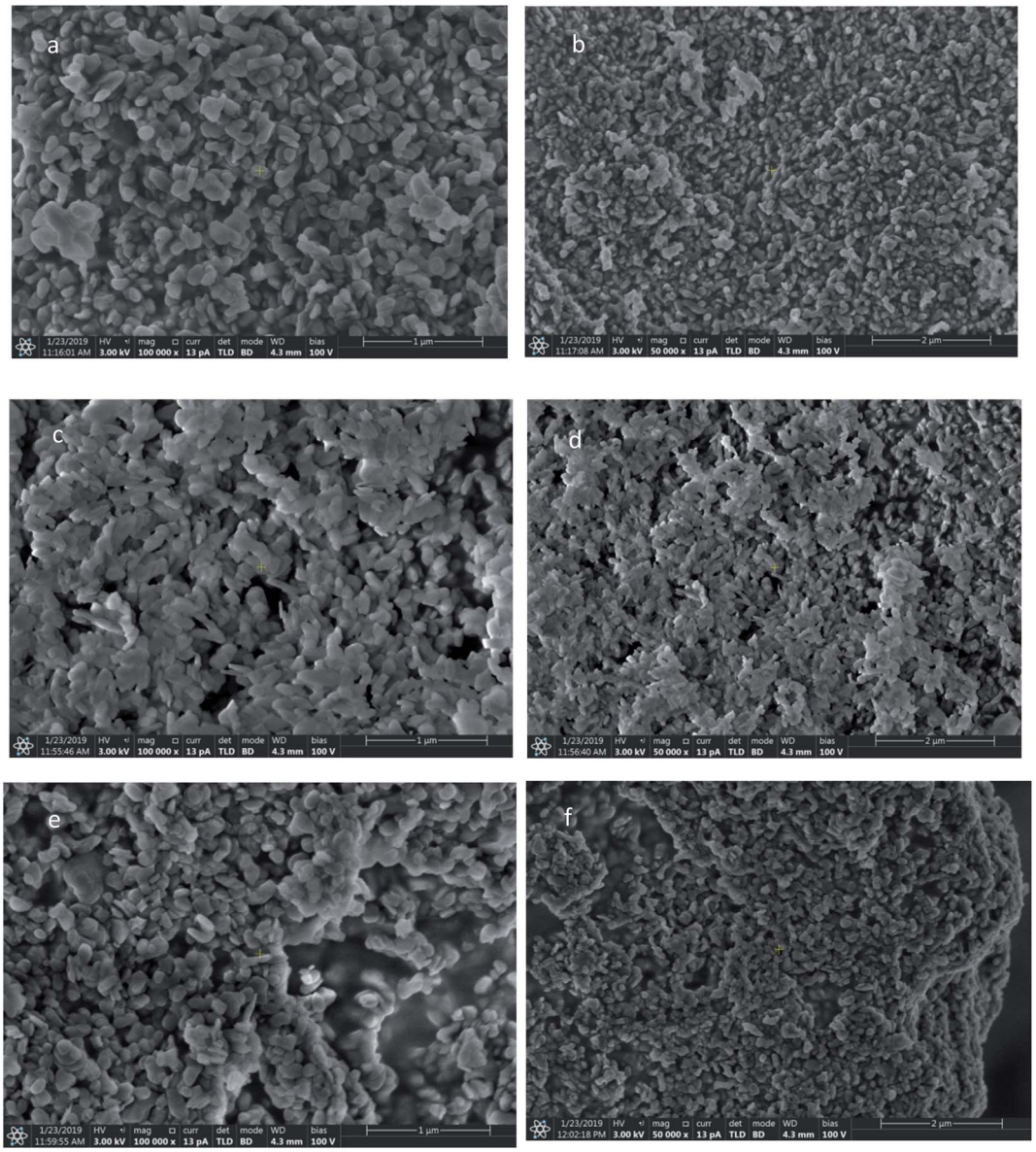

Fig. 2 SEM images of ZnMgAl-LDHs (a and b), ZnMgAl-MMO (c and d) and 65PEG/MMO (e and f).

3.3 Characterization by XRD

The XRD patterns of PEG, ZnMgAl-LDHs, ZnMgAl-MMO and 65PEG/MMO are presented in Fig. 3. Two sharp peaks at 19.18° and 23.30° represent a typical crystalline structure of PEG. The characteristic phases of ZnMgAl-LDHs can be observed at around 11.65° (003), 23.42° (006), and 34.88° (009), respectively. In the case of ZnMgAl-MMO, upon calcination at 500 °C, all the typical hydrotalcite peaks disappeared suggesting that the hydrotalcite structures were destroyed. The occurrence of new peaks approximately at 2θ of 34.28°, 36.10°, 43.0° and 62.8° matches well with the standard phase of ZnO and MgO and no definite reflections of aluminium oxides were discerned. For 65PEG/MMO PCM, well-crystalized PEG was obviously found in XRD patterns while the characteristic phase of ZnMgAl-MMO also remained. This observation suggests that 65PEG/MMO PCM owns a composite structure of which the crystal state of PEG is not affected by the incorporation of ZnMgAl-MMO.

3.4 Characterization by FTIR

Fig. 4 presents the FTIR spectra of PEG, ZnMgAl-LDHs, ZnMgAl-MMO and 65PEG/MMO PCM. In the case of PEG, the absorption bands at 946 and 2880 cm^{-1} correspond to the $-CH_2$ stretching vibration of PEG; the broad peak at around 3400 cm^{-1} represents the stretching vibration of terminal hydroxyl group; and the peaks at 1110 cm^{-1} and 1145 cm^{-1} belong to the vibration range of C–O–C. Typical bands of LDHs are at 3000–3600 cm^{-1} (–OH stretching), 1620 cm^{-1} (the interlayer water bending), and 1365 cm^{-1} (O–C–O stretching), while some spectra at the low band are M–O stretching modes. Owing to the calcination at 500 °C, the FTIR spectra of ZnMgAl-MMO display the weakened characteristic bands of –OH and CO_3^{2-}. The characteristic

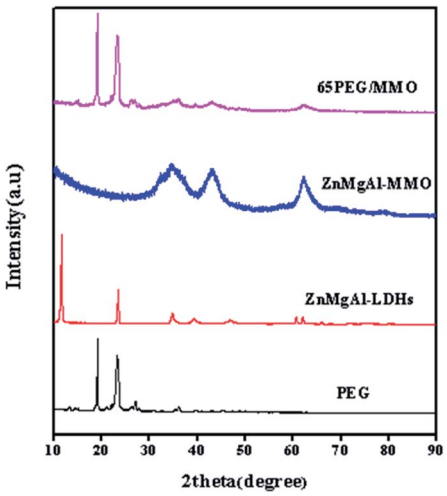

Fig. 3 XRD patterns of PEG, ZnMgAl-LDHs, ZnMgAl-MMO, and 65PEG/MMO.

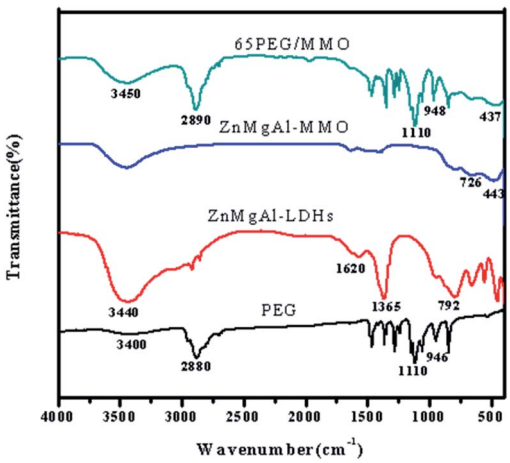

Fig. 4 FTIR spectra of PEG, ZnMgAl-LDHs, ZnMgAl-MMO, and 65PEG/MMO.

peaks at 443 cm^{-1} and 726 cm^{-1} were observed suggesting the appearance of the Zn–O and Mg–O stretching modes. These features indicate a great distortion of the LDHs laminar structures. For 65PEG/MMO PCM, the characteristic peaks for both ZnMgAl-MMO and PEG were observed and no new absorption peaks could be obviously found. Nevertheless, compared to the FTIR spectra of both pristine ZnMgAl-MMO and PEG, a little shift of the characteristic peaks were found indicating that physical absorption was probably the main interaction mechanism between ZnMgAl-MMO and the function groups of PEG. In a sum, all above observations revealed that no chemical reactions had occurred during the preparation of PEG/MMO PCM and physical interaction played a vital role in shaping the melted PEG.

3.5 Thermal properties of PEG/MMO PCM

Thermal property of PEG and 65PEG/MMO PCM was evaluated by DSC analysis and the result is shown in Fig. 5 and Table 2. It

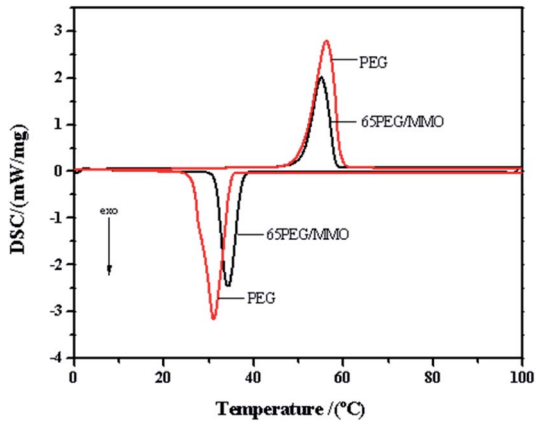

Fig. 5 DSC curves of PEG and 65PEG/MMO.

can be observed from Fig. 5 that the phase change curves of PEG and 65PEG/MMO PCM are similar other than the values of phase change temperature and latent heat during the heating and cooling cycles. By numerical integration of the area under the melting and crystallization peak respectively, the latent heat of melting and crystallization was calculated to be 185.4 J g^{-1} and 184.8 J g^{-1} for PEG and 108.1 J g^{-1} and 107.9 J g^{-1} for 65PEG/MMO PCM, respectively (Table 2). For 65PEG/MMO PCM, the theoretic latent heat of melting and crystallization as calculated from pristine PEG is 120.51 J g^{-1} and 120.12 J g^{-1} (185.4 × 65% = 120.51 J g^{-1}, 184.8 × 65% = 120.12 J g^{-1}). Comparing to the actual and theoretic latent heat of melting and crystallization, a fact can be obtained that the PEG in 65PEG/MMO PCM had not been completely crystallized, and the crystallization percentage was calculated to be 89.7% and 89.8% in melting and crystallization respectively (108.1/120.51 = 89.7%, 107.9/120.12 = 89.8%). The partial crystallization can be attributed to the interaction between ZnMgAl-MMO and PEG resulting in small parts of the PEG under the "partially confined state" and thus a different crystallization behavior.

As shown in Fig. 5 and Table 2, the starting temperature (T_{ms}), the peak temperature (T_{mp}) and the end temperature (T_{me}) of melting of 65PEG/MMO PCM is 50.9 °C, 55.2 °C and 58.2 °C respectively, which is slightly less than those of the pristine PEG (51.0 °C, 56.3 °C, 59.3 °C). The starting temperature (T_{cs}), the peak temperature (T_{cp}) and the end temperature (T_{ce}) of the crystallization of 65PEG/MMO PCM is 37.4 °C, 34.4 °C and 31.7 °C respectively, which is higher than those of the pristine PEG (34.9 °C, 31.2 °C, 26.3 °C). These suggest that the physical interaction between ZnMgAl-MMO and PEG restrains phase change behavior, or affects the thermal conductivity of 65PEG/MMO PCM.[19,46] Moreover, the difference between the melting and crystallization temperature, also known as the extent of supercooling, is smaller for 65PEG/MMO PCM compared with that for pristine PEG, which is believed to be advantageous in practical application.[21]

Appropriate phase change temperature with substantial latent heat is one of the most important considerations for bitumen pavement constructed with PCM, which is supposed to be very beneficial to reduce the diseases caused by extreme high

Table 2 Thermal properties of PEG and 65PEG/MMO PCM[a]

Sample	H_m (J g^{-1})	T_{ms} (°C)	T_{mp} (°C)	T_{me} (°C)	P_m (%)	H_c (J g^{-1})	T_{cs} (°C)	T_{cp} (°C)	T_{ce} (°C)	P_c (%)
PEG	185.4	51.0	56.3	59.3		184.8	34.9	31.2	26.3	
65PEG/MMO	108.1	50.9	55.2	58.2	89.7	107.9	37.4	34.4	31.7	89.8

[a] Note: H_m = latent heat of melting, H_c = latent heat of crystallization; P_m = the melting crystallization fraction of the PEG, P_c = the crystallization fraction of the PEG; T_{ms} = starting melting temperature, T_{mp} = peak melting temperature, T_{me} = end melting temperature; T_{cs} = starting crystallization temperature, T_{cp} = peak crystallization temperature, T_{ce} = end crystallization temperature.

or low temperatures.[12,47] As previously described, the starting melting temperature of 65PEG/MMO PCM is 50.9 °C, which matches well with bitumen's softening point (about 50 °C). That is to say when ambient temperature reaches 50.9 °C, the phase change process of 65PEG/MMO PCM starts with absorbing and storing energy. The phase change in turn would slow down the process for bitumen pavement in reaching the peak temperature achieving the "peak elimination" effect.[48] On the other hand, when ambient temperature drops to the starting crystallization temperature (37.4 °C), 65PEG/MMO PCM releases the energy exerting the "valley filling" effect.[48] Furthermore, the latent heat of melting and freezing of 65PEG/MMO PCM which is 108.1 J g^{-1} and 107.9 J g^{-1} respectively is considerable. Therefore, it is promising for the application of PEG/MMO PCM for thermoregulation in bitumen pavement.

3.6 Thermal stability of PEG/MMO PCM

Fig. 6 displays three TG curves of PEG, MMO and 65PEG/MMO PCM. As can be seen from the curves, there are no obvious degradation for MMO in the range of 25 °C to 600 °C, while the main mass loss step of PEG starts at about 315 °C and ended at 430 °C due to the decomposition of PEG chain. The degradation of 65PEG/MMO PCM is observed at the temperature range of 25 °C to 600 °C which is roughly consistent with the thermal behavior of PEG. These results revealed that 65PEG/MMO PCM owned good thermal stability and could be used repeatedly below 300 °C. In the construction of bitumen pavement, the maximum operating temperature of bitumen mixture is usually below 180 °C, so the thermal reliability of PEG/MMO PCM in bitumen pavement can be certainly guaranteed.

3.7 UV-vis absorbance of PEG/MMO PCM

Fig. 7 presents the UV-vis absorbance spectra of PEG and 65PEG/MMO PCM. As can be seen, the absorption intensity of 65PEG/MMO PCM is stronger than that of PEG, especially in the ultraviolet region. Compared to the weak absorption peak at 250 nm for PEG, 65PEG/MMO PCM gives a stronger absorption intensity and a broader wavelength extending to be around 330 nm, which is due to the existence of ZnO and the coupling interaction among ZnO, MgO and Zn–Al composite oxides in ZnMgAl-MMO.[36,45] In addition, a relevant NMR research revealed that in the case of ZnMgAl-MMO composite, not only Al affected the band structure of ZnO crystal, but also the dipole moment changed.[49] These factors can also enhance the ultraviolet absorption property of ZnMgAl-MMO. Moreover, no obvious evidence showed that the property of ZnMgAl-MMO was affected during the preparation of PEG/MMO PCM. In this regard, it can be expected that adding 65PEG/MMO PCM into bitumen, would not only offer thermal regulation capacity but also improve UV aging resistance of the bitumen pavement.

3.8 Conventional physical property of PEG/MMO PCM modified bitumen

Table 3 lists the physical properties of base bitumen and modified bitumen. The results show that the addition of PEG/MMO PCM increases the softening point and viscosity and

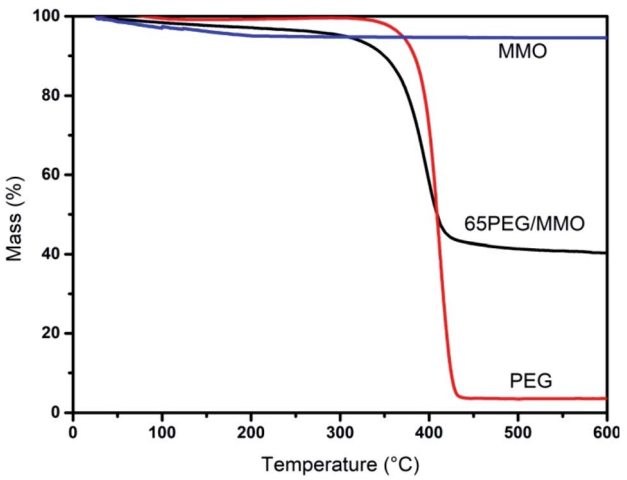

Fig. 6 TG curves of PEG, MMO and 65PEG/MMO.

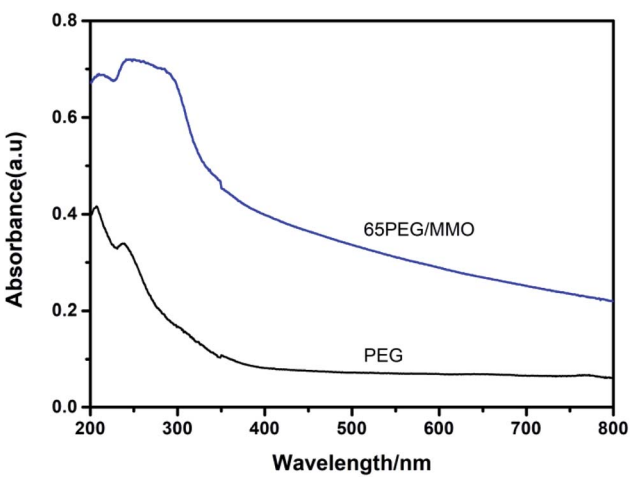

Fig. 7 UV absorption of PEG and 65PEG/MMO.

Table 3 The physical properties of base bitumen and modified bitumen

Physical properties	BB	PMB
Penetration (25 °C, 0.1 mm)	61.5	60.6
Softening point (°C)	50.1	51.0
Ductility (10 °C, cm)	10.6	10.8
Viscosity (135 °C, Pa s)	0.451	0.531

decreases the penetration of bitumen, while it has little influence on ductility. PMB exhibits the larger softening point and viscosity, the smaller penetration compared with BB, indicating the addition of PEG/MMO PCM can improve the high temperature performance of bitumen.

3.9 Thermal regulation of PEG/MMO PCM modified bitumen

The thermal regulation of PEG/MMO PCM modified bitumen was evaluated by comparing the thermal energy storage and release performance of PMB with that of BB. The thermal energy storage and release curves of BB and PMB are shown in Fig. 8. It can be seen that during heating period, the temperature rising rate of PMB is lower than that of BB especially in the range of 45–65 °C. The temperature of PMB is consistently lower than that of BB and the maximal temperature difference is 5.1 °C between BB and PMB. In addition, as can be seen from the curves, the temperature of BB and PMB starts from 18.1 °C in the beginning. It takes 3950 s for BB to reach the equilibrium temperature of 75 °C, while 4270 s for PMB. On the other hand, during the cooling period, it is clear that the temperature dropping of PMB is slower than that of BB particularly in the range of 40–30 °C. The temperature of PMB is consistently higher than that of BB and the maximal temperature difference is 4.5 °C between BB and PMB. The results indicated that the addition PEG/MMO PCM into base bitumen effectively lowered the rate of temperature variation of base bitumen, and then shortened the duration of high temperature and postponed the emergence of extreme temperature. The thermoregulation was attributed to the phase change capacity for heat storage and release as well as the thermal conductivity change of PEG/MMO PCM. Therefore, PEG/MMO PCM modified bitumen is believed to play an important role in eliminating peak temperature and filling valley temperature of bitumen pavements, and mitigate the diseases caused by extreme temperature.

3.10 UV aging resistance of PEG/MMO PCM modified bitumen

Bitumen is liable to hard and brittle under the UV radiation, which can induce premature deterioration of bitumen pavement.[50] It has been found that the important change was the increase of oxidation components especially carbonyl and sulfoxide during UV aging of bitumen. Therefore, the aging extent of bitumen can be evaluated by quantifying the content variation of oxygenated functional groups which can be characterized by FTIR.[51,52] Carbonyl index ($I_{C=O}$) and sulfoxide index ($I_{S=O}$) are used to evaluate the content of carbonyl group (C=O) and sulfoxide group (S=O) and could be defined by the following equations:[53,54]

$$I_{CaO} = \frac{\text{area of carbonyl band centered around } 1700\ \text{cm}^{-1}}{\sum \text{area of spectral bands between } 2000\ \text{cm}^{-1} \text{ and } 600\ \text{cm}^{-1}}$$

$$I_{SaO} = \frac{\text{area of carbonyl band centered around } 1030\ \text{cm}^{-1}}{\sum \text{area of spectral bands between } 2000\ \text{cm}^{-1} \text{ and } 600\ \text{cm}^{-1}}$$

Fig. 9 gives the FTIR spectra of BB and PMB before and after UV aging. The corresponding structural indices are shown in

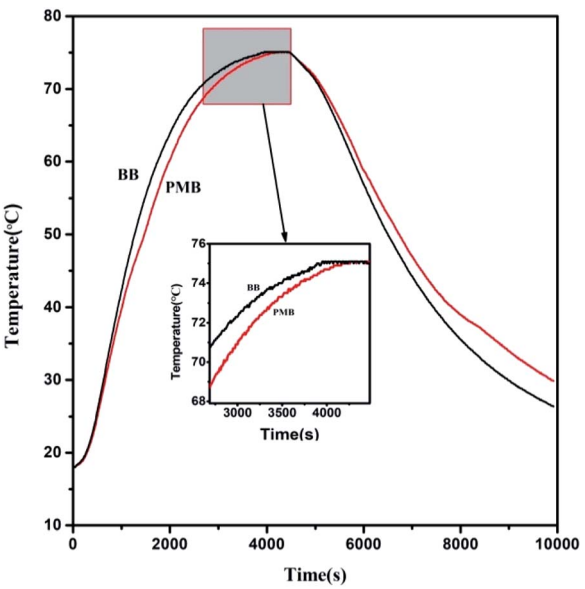

Fig. 8 Thermal energy storage and release curves of BB and PMB.

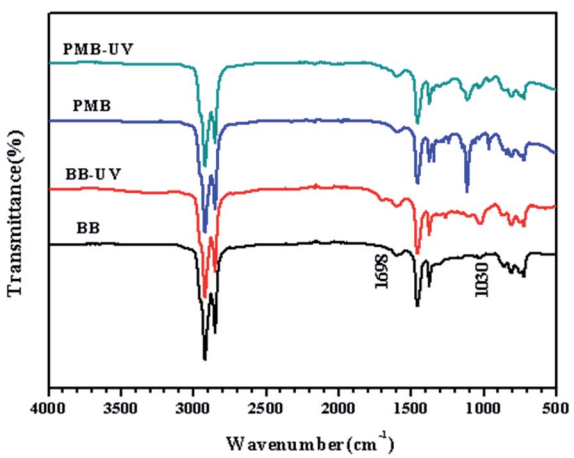

Fig. 9 FTIR spectra of base and modified bitumen after aging.

Table 4 Structural indexes of base and modified bitumen before and after UV aging

Sample	$I_{C=O}$	ΔI_C	$I_{S=O}$	ΔI_S
BB	0		0.024	
BB-UV	0.029	0.029	0.102	0.078
PMB	0		0.020	
PMB-UV	0.012	0.012	0.042	0.022

Table 4. As can be seen in Fig. 9, the absorbance peaks at around 1698 cm^{-1} correspond to the formation of C=O stretch in carbonyl group, while those at 1030 cm^{-1} correspond to the formation of S=O stretch in sulfoxides group. It can be seen that the C=O stretch peaks at 1698 cm^{-1} of BB and PMB are almost imperceptible before UV aging. However, both BB and PMB show stretch bands at 1698 cm^{-1} after UV aging and the band area of BB is obviously greater than that of PMB. The change of the S=O stretch peaks at 1030 cm^{-1} of BB and PMB before and after UV aging is in accordance with that of the C=O stretch peaks, although the S=O stretch peaks appear before UV aging. The differences of the structural index before and after aging (ΔI_C, ΔI_S) were used for quantitatively evaluating the influence extent on bitumen during aging. As can be seen from Table 4, the differences of both $I_{C=O}$ and $I_{S=O}$ values for BB and PMB before UV aging are neglectable. This indicates that 65PEG/MMO PCM has little influence on the C=O and S=O of bitumen before aging. However, both $I_{C=O}$ and $I_{S=O}$ values of BB and PMB are visibly increased after UV aging, and both ΔI_C and ΔI_S values of PMB are smaller than those of BB, indicating a less serious aging of PMB than BB. That is to say PMB has a better UV aging resistance property than BB owing to the restrainment of the oxidation of bitumen during UV aging by 65PEG/MMO PCM, and thus help alleviate the deterioration of bitumen.

High energy UV light can easily break the chemical bonds of bitumen to form free radical, which is extremely unstable at the presence of oxygen. Then the oxidation reaction of bitumen is apt to happen when the bitumen material is exposed to the atmosphere.[54] As it is well-known that ZnO is an excellent UV absorber for effectively attenuating (absorb and/or scatter) UV radiation in the UVB (290–320 nm) and in the UVA (320–400 nm) range. Compared to a commercial ZnO material, the higher visible light transmittance and higher UV blocking absorption of ZnO-based MMO materials (derived from calcination of the LDHs precursor in this study) can be attributed to the high dispersion of the ZnO phase within the amorphous aluminum oxide phase.[35] Therefore, the PEG/MMO PCM added in bitumen could attenuate the UV lights effectively and thus restrain the oxidation of bitumen.

4. Conclusions

In this study, a new PEG/MMO form-stable PCM was successfully synthesized using a melting impregnation method. PEG and ZnMgAl-MMO which obtained from the calcination of ZnMgAl-LDHs, was adopted as the PCM and supporting matrix, respectively. Due to physical adsorption and capillary forces, the movement of PEG was confined resulting in the stabilization of PEG/MMO PCM during phase transition. The maximum weight fraction of PEG confined in the ZnMgAl-MMO without leakage was found to be 65%.

XRD and FTIR analysis revealed that no chemical reaction occurred between PEG and MMO, and the properties of both PEG and MMO were not impacted during the synthesis. DSC results indicated the melting and freezing starting temperatures of 65PEG/MMO PCM were 50.9 °C and 37.4 °C, and the melting and freezing enthalpy were 108.1 J g^{-1} and 107.9 J g^{-1}, respectively. The increased UV absorption capacity of 65PEG/MMO PCM was confirmed by UV-vis absorbance spectra analysis.

The thermal storage and release test and accelerated UV irradiation aging test of bitumen samples modified by 65PEG/MMO PCM verified its promising temperature regulation and UV aging resistance properties. As a new type of performance-enhancing additive, PEG/MMO PCM is expected to be effective in regulating extreme temperature and resisting UV aging of bitumen and thus could significantly extend the service life of bitumen pavement.

Conflicts of interest

There are no conflicts of interest to declare.

Acknowledgements

This work was supported by Minjiang Scholar program of Fujian Province, China (GXRC-19045), and Natural Science Foundation of Fujian Province (grant number 2019J01235). CCCC Second Harbour Engineering Co., Ltd. Fuzhou Subsidiary Company is also greatly acknowledged for the support with a joint project (No. 00501901).

References

1 B. Ma, S. Adhikari, Y. Chang, J. Ren, L. Jiang and Z. You, *Constr. Build. Mater.*, 2013, **42**, 114–121.
2 B. Athukorallage, T. Dissanayaka, S. Senadheera and D. James, *Constr. Build. Mater.*, 2018, **164**, 419–432.
3 S. Sundararajan, A. B. Samui and P. S. Kulkarni, *J. Mater. Chem. A*, 2017, **5**, 18379–18396.
4 J. Wang, Y. Mu, Y. Lu, Z. Jin, T. Li, H. Gao, F. Shuang, W. Dong and W. Ge, *Nano Energy*, 2016, **19**, 78–87.
5 D. W. Hawes and D. Feldman, *Sol. Energy Mater. Sol. Cells*, 1992, **27**, 91–101.
6 A. M. Khudhair and M. M. Farid, *Energy Convers. Manage.*, 2004, **45**, 263–275.
7 M. Kheradmand, J. Castro-Gomes, M. Azenha, P. D. Silva, J. L. B. D. Aguiar and S. E. Zoorob, *Constr. Build. Mater.*, 2015, **89**, 48–59.
8 T. Silva, R. Vicente, N. Soares and V. Ferreira, *Energy Build.*, 2012, **49**, 235–245.

9 T. C. Ling and C. S. Poon, *Constr. Build. Mater.*, 2013, **46**, 55–62.
10 B. L. Gowreesunker and S. A. Tassou, *Build. Environ.*, 2013, **59**, 612–625.
11 J. Jin, F. Lin, R. Liu, T. Xiao, J. Zheng, G. Qian, H. Liu and P. Wen, *Sci. Rep.*, 2017, **7**, 16998.
12 J. Ren, B. Ma, S. Wei, X. Zhou and L. Chao, *Constr. Build. Mater.*, 2014, **71**, 53–62.
13 M. Chen, W. Lu and J. Lin, *J. Test. Eval.*, 2012, **40**, 20120091.
14 X. Bian, Y. Q. Tan, J. F. Lv and L. Y. Shan, *Adv. Eng. Forum*, 2012, **5**, 322–327.
15 B. Ma, S. S. Wang and J. Li, *Adv. Mater. Res.*, 2011, **168–170**, 2625–2630.
16 M. Z. Chen, J. Hong, S. P. Wu, W. Lu and G. J. Xu, *Adv. Mater. Res.*, 2011, **219–220**, 1375–1378.
17 L. He, J. Li, C. Zhou, H. Zhu, X. Cao and B. Tang, *Sol. Energy*, 2014, **103**, 448–455.
18 B. Tang, J. Cui, Y. Wang, C. Jia and S. Zhang, *Sol. Energy*, 2013, **97**, 484–492.
19 T. Qian, J. Li, H. Ma and Y. Jing, *Sol. Energy Mater. Sol. Cells*, 2015, **132**, 29–39.
20 H. Yang, L. Feng, C. Wang, Z. Wei and X. Li, *Eur. Polym. J.*, 2012, **48**, 803–810.
21 S. Karaman, A. Karaipekli, A. Sarı and A. Biçer, *Sol. Energy Mater. Sol. Cells*, 2011, **95**, 1647–1653.
22 T. Qian, J. Li and Y. Deng, *Sci. Rep.*, 2016, **6**, 32392.
23 A. Sarı, *Energy Build.*, 2014, **69**, 184–192.
24 E. Onder, N. Sarier, G. Ukuser, M. Ozturk and R. Arat, *Thermochim. Acta*, 2013, **566**, 24–35.
25 A. R. Bahramian, L. S. Ahmadi and M. Kokabi, *Iran. Polym. J.*, 2014, **23**, 163–169.
26 C. Wang, L. Feng, W. Li, J. Zheng, W. Tian and X. Li, *Sol. Energy Mater. Sol. Cells*, 2012, **105**, 21–26.
27 L. Zhang, H. Shi, W. Li, H. Xu and X. Zhang, *Polym. Int.*, 2014, **63**, 982–988.
28 L. Feng, Z. Jie, H. Yang, Y. Guo, L. Wei and X. Li, *Sol. Energy Mater. Sol. Cells*, 2011, **95**, 644–650.
29 E.-Y. Ding, Y. Jiang and G.-K. Li, *J. Macromol. Sci., Part B: Phys.*, 2001, **40**, 1053–1068.
30 C. Alkan, E. Günther, S. Hiebler and M. Himpel, *Energy Convers. Manage.*, 2012, **64**, 364–370.
31 X. H. Liang, Y. Q. Guo, L. Z. Gu and E. Y. Ding, *Macromolecules*, 1995, **28**, 6551–6555.
32 S. B. Sentürk, D. Kahraman, C. Alkan and Ï. Gökce, *Carbohydr. Polym.*, 2011, **84**, 141–144.
33 S. Zhu, T. Ji, B. Yang and Z. Yang, *RSC Adv.*, 2019, **9**, 23435–23443.
34 F. Cavani, F. Trifirò and A. Vaccari, *ChemInform*, 2010, **23**, 173–178.
35 X. Zhao, F. Zhang, S. Xu, D. G. Evans and D. Xue, *Chem. Mater.*, 2010, **22**, 3933–3942.
36 X. Yuan, Q. Jing, J. Chen and L. Li, *Appl. Clay Sci.*, 2017, **143**, 168–174.
37 W. R. D. Carmo, J. Fischer-Haddad, L. H. Chagas, M. S. S. Beltrão, G. S. G. D. Carvalho, L. C. A. D. Oliveira, T. E. Souza, A. A. Leitão and R. Diniz, *Appl. Clay Sci.*, 2015, **116–117**, 31–38.
38 J. S. Valente, J. Hernandez-Cortez, M. S. Cantu, G. Ferrat and E. López-Salinas, *Catal. Today*, 2010, **150**, 340–345.
39 J. S. Valente, F. Tzompantzi, J. Prince, J. G. H. Cortez and R. Gomez, *Appl. Catal., B*, 2009, **90**, 330–338.
40 C. Alanis, R. Natividad, C. Barrera-Diaz, V. Martínez-Miranda, J. Prince and J. S. Valente, *Appl. Catal., B*, 2013, **140**, 546–551.
41 D. Pan, S. Ge, J. Zhao, Q. Shao and Z. Guo, *Dalton Trans.*, 2018, **47**, 9765–9778.
42 L. Zou, F. Li, X. Xiang, D. G. Evans and X. Duan, *Chem. Mater.*, 2006, **18**, 5852–5859.
43 E. M. Seftel, E. Popovici, M. Mertens, K. D. Witte, G. V. Tendeloo, P. Cool and E. F. Vansant, *Microporous Mesoporous Mater.*, 2008, **113**, 296–304.
44 X. Cheng, X. Huang, X. Wang and D. Sun, *J. Hazard. Mater.*, 2010, **177**, 516–523.
45 L. Zhang, C. H. Dai, X. X. Zhang, Y. N. Liu and J. H. Yan, *Trans. Nonferrous Met. Soc. China*, 2016, **26**, 2380–2389.
46 J. Li, L. He, T. Liu, X. Cao and H. Zhu, *Sol. Energy Mater. Sol. Cells*, 2013, **118**, 48–53.
47 Y. B. Zhang, H. Z. Zhu, L. I. Jing-Ruo and H. E. Li-Hong, *J. Zhengzhou Univ.*, 2012, **33**, 10–14.
48 H. H. Li, R. L. Jing and Z. Z. Hong, *Appl. Mech. Mater.*, 2013, **357–360**, 1277–1281.
49 L. Li, C. Y. Zhang and X. Duan, *J. Beijing Univ. Chem. Technol.*, 2002, **29**, 83–87.
50 P. Cong, L. Ning, T. Yu and Y. Zhang, *Constr. Build. Mater.*, 2016, **123**, 534–540.
51 Z. G. Feng, S. J. Wang, H. J. Bian, Q. L. Guo and X. J. Li, *Constr. Build. Mater.*, 2016, **115**, 48–53.
52 J. Lamontagne, P. Dumas, V. Mouillet and J. Kister, *Fuel*, 2001, **80**, 483–488.
53 Z.-G. Feng, J.-Y. Yu, H.-L. Zhang, D.-L. Kuang and L.-H. Xue, *Mater. Struct.*, 2013, **46**, 1123–1132.
54 X. Song, J. Yu, Y. Sun and S. Wu, *Mater. Chem. Phys.*, 2015, **152**, 54–61.